




Taurolidine inhibits influenza virus infection and prevents influenza-induced cytokine storm, vasoconstriction and lung damage

Chaoxiang Lv^{1,2,3} · Jin Guo^{2,4} · Rongbo Luo² · Yuanguo Li² · Bingshuo qian^{2,5} · Xiaopan Zou⁶ · Tiecheng Wang² · Beilei Shen² · Weiyang Sun² · Yuwei Gao^{2,4,7} 

Received: 12 January 2025 / Revised: 12 January 2025 / Accepted: 21 February 2025
© The Author(s) 2025

Abstract

Influenza virus causes worldwide outbreaks and seasonal epidemics, posing a severe threat to public health and social development. Effective prevention and treatment of influenza infections remain major challenge for global healthcare. In this study, we observed that taurolidine effectively inhibited the proliferation of several human or animal influenza virus strains and protected mice from lethal-infection. Taurolidine treatment decreased the viral titer in the lungs of infected mice, reduced the ratio of immune cells, and alleviated lung pathology. Additionally, taurolidine treatment attenuated the rise of blood pressure, pulse wave velocity, and pulmonary aortic thickness in a mouse model for influenza virus infection. We also found that taurolidine significantly decreased intracellular Ca^{2+} concentration and effectively alleviated pulmonary artery vasoconstriction during influenza virus infection. Mechanistically, we observed that vascular smooth muscle contraction signaling pathway was significantly enriched, and taurolidine inhibited the activation of the MLCK/p-MLC pathway. Taking together, these findings confirm the effectiveness of taurolidine as an antiviral agent and highlight its important roles in mitigating host immune cell infiltration and vasoconstriction induced by influenza virus infection.

Keywords Taurolidine · Vasoconstriction · Influenza virus · Calcium influx · MLCK/p-MLC signaling pathway

Introduction

The influenza virus is the primary cause of acute respiratory infections and seasonal influenza, which can easily trigger seasonal outbreaks and pandemics, posing a significant threat to public health and social development [1–3]. Presently, vaccination and antiviral treatments serve as the main preventive and supportive measures for managing influenza pandemic [4]. However, vaccines are limited in their ability to identify pandemic strains, and resistance to existing class of direct-acting antivirals (DAAs), like adamantane (the M2 inhibitor), oseltamivir (the NA inhibitor) and baloxavir (the PA inhibitor) has become widespread [5]. Meanwhile, host-targeted therapies, anti-inflammatory drugs, and immunomodulators have also shown broad-spectrum antiviral activity against influenza viruses [2]. In addition, the current ability of vaccines to identify pandemic strains is limited. These challenges underscore the urgent need to develop new antiviral strategies with new mechanisms of action to reduce the possibility of drug resistance [6].

Inflammatory cytokines are markedly elevated following influenza virus infection, leading to a “cytokine storm”,

✉ Yuwei Gao
yuwei0901@outlook.com

¹ The Research Center for Preclinical Medicine, Southwest Medical University, Luzhou 646000, China

² Changchun Veterinary Research Institute, Chinese Academy of Agricultural Sciences, Changchun 130122, China

³ School of Basic Medical Sciences, Southwest Medical University, Luzhou 646000, China

⁴ College of Life Sciences, Shandong Normal University, Jinan 250358, China

⁵ School of Pharmacy, Henan University, Kaifeng 475004, China

⁶ Breast and Thyroid Surgery, Jilin Province People's Hospital, Changchun, Jilin 130021, China

⁷ Changchun Veterinary Research Institute, Chinese Academy of Agricultural Sciences, Changchun, Jilin 130122, China

which is hypothesized to be the main cause of mortality [7]. The cytokine storm can result in the accumulation of excessive immune cells and viscous secretions in lung tissues, thereby obstructing gas exchange and ultimately leading to death [8]. A study has shown that the “cytokine storm”, characterized by the overproduction and dysfunction of inflammatory cytokines, is a major cause of host death after influenza virus infection [9]. This indicates that severe lung inflammation is related to lung tissue pathologies, such as lung tissue edema, infectious pneumonia, and alveolar hemorrhage [10]. Consequently, it is essential to maintain the host’s antiviral response as an optimal defense mechanism against influenza virus infection.

The vascular smooth muscle system drives blood flow, cytokine release, and immune cell recruitment by regulating the balance between vasoconstriction and vasodilatation [11]. The contraction of vascular smooth muscle is regulated by a voltage- and calcium-dependent process (called excitation-contraction coupling) in response to neuronal stimulation [12]. Additionally, vasomotor control is the basis for the acute and rapid adaptation of blood vessel diameter, which is mainly due to the vasoconstriction caused by the active contraction of vascular smooth muscle cells. Changes in vascular structure represent the dynamic processes associated with chronic hemodynamic alternations [13]. The acute regulation of blood vessel diameter and the consequent vascular resistance depend on the activation state of the contraction mechanism involving actin, specifically the interaction of actin in the vascular smooth muscle cells [14]. The alteration of Ca^{2+} flux and membrane potential regulate the phosphorylation of myosin-light-chains (MLCs) and the actin-myosin cross-bridge cycles, ultimately leading to rapid vasoconstriction [15], which is a critical mechanism for the host’s adaptation to a rapid immune response.

Taurolidine, a derivative of the amino acid taurine, has been found to possess anti-endotoxin, anti-bacterial and anti-adhesion properties [16]. Its mechanism of action involves inhibiting microbial adhesion through chemical reactions with cell walls, including bacterial and fungus [17]. Additionally, previous studies have shown that taurolidine inhibits the synthesis of cytokines (IL-1 and TNF) in human peripheral blood mononuclear cells [18], which indicates that taurolidine may play important roles in cytokine-induced immune responses and related diseases. Despite these findings, the antiviral effectiveness of taurolidine remains unclear.

Here, we explored the anti-influenza virus activity of taurolidine both *in vitro* and *in vivo*. Using genomics and chemical tools, we defined the important role of taurolidine in attenuating the inflammation response. Furthermore, we revealed that the suppression of vasoconstriction signaling pathway through taurolidine treatment can reduce mortality

in mice infected with the influenza virus. Therefore, the vasoconstrictor signal provides a mechanism to reduce influenza virus-induced incidence and revealed the unforeseen role of taurolidine as a modulator of the inflammatory response and vasoconstriction.

Materials and methods

Antibodies, mice, reagents and viruses

Antibodies against viral nucleoprotein (virus NP, ab20343), AT1R (cat no. ab124505), CaM (cat no. ab2860), and MLCK (ab236299) were provided by Abcam (Burlington, CA, USA). The antibodies against MLC (Loc:3672) and p-MLC (Loc:3675) were purchased from Cell Signaling Technology (Beverly, MA, USA). Taurolidine, oseltamivir (PHR1781), and the antibody against β -actin were obtained from Sigma-Aldrich (St. Louis, MO, USA). The MLCK inhibitor ML-7 HCL (S8388) and ML-9 HCL (S6847) were purchased from Selleck (Houston, TX, USA). Six- to eight-week-old BALB/c female mice derived from Charles River Laboratory Animal Technology Co., Ltd (Beijing, China). Influenza A viruses (IAV/H1N1-UI182, IAV/H1N1-PR8, IAV/H3N2) originated from the Institute of Changchun Veterinary Research, Chinese Academy of Agricultural Sciences (Changchun, China) [19, 20]. Influenza B virus strains (IBV/S9-MD) were rescued according to the sequence of B/Yamagata/16/88 (GenBank accession: CY018765-CY018772) and passaged in mice to get mouse-adapted strains. All experiments with influenza viruses were performed in a biosafety level 2 (BSL-2) laboratory in Changchun Veterinary Research Institute.

Cell culture

The Madin-Darby canine kidney (MDCK) cell line, the human type-II alveolar epithelial (A549) cell line, and the vascular smooth muscle cells (VSMCs) were cultured in Dulbecco’s modified Eagle’s medium (DMEM) supplemented with 10% fetal bovine serum (FBS, Gibco, 10091148) along with 100 U/mL penicillin and 100 $\mu\text{g/mL}$ streptomycin. All cells were cultured at 37 °C and 5% CO_2 in humidified air.

Virus infection and drug inhibitory efficacy

All virus strains were passaged and titrated on cells at the designated multiplicity of infection (MOI). Three different infection regimens were used to evaluate the active stages of taurolidine against influenza viruses, such as pre-treatment (virus was added to the cells after 15 min of co-incubation

with taurolidine), co-treatment (virus was added to the cells after 15 min of co-incubation with taurolidine), and post-treatment (taurolidine was added to the cells for a 4 h treatment after virus infection). Taurolidine was solubilized in PBS at a concentration of 4 mg/ml, and a series of dilutions of taurolidine (0, 5, 10, 25, 50, 100 and 200 µg/mL) were added 4 h post-infection. We followed the previous method to assess drug inhibitory efficacy *in vivo* [21].

Plaque, hemagglutination (HA) test and cytotoxicity assay

MDCK cells were infected with 40 PFU/well of influenza virus. Following adsorption of the virus for 2 h, the inoculum was removed, and the cells were overlaid with DMEM containing 1.5% agarose with serial dilutions of PG. After 72 h, they were stained, and images were captured. For the hemagglutination experiment, MDCK cells infected with influenza virus were divided into different groups, including DMEM-treated group (0 µg/mL), taurolidine-treated groups (5 µg/mL, 25 µg/mL, 50 µg/mL), and oseltamivir-treated groups (5 µg/mL, 25 µg/mL, 50 µg/mL). The cell supernatant (50 µL) from each group was collected and added to a 96-well micro-hemagglutination plate after 48 h of treatment. Subsequently, 50 µL of a 1% chicken red blood cell (RBC) suspension was added to each well. After standing at room temperature for 15 min, the results were observed. Cytotoxicity was assayed by the MTT assay (Promega). The cells were plated in 96-well plates (48000 cells per well) and cultured for 48 h, and then the cells growth was detected according to the instructions of manufacturer. Briefly, 10 µL of MTT solution was added to each well, and the absorbance of each well was measured Spectro-photometrically at 570 nm after incubating for 4 h. We conducted three independent cell experiments, with three replicate wells for each treatment group in each experiment.

Neuraminidase detection assay

According to the manufacturer's instructions (P0306, Beyotime, China), the 96-well fluorescein label plate was added with 70 µL of neuraminidase detection buffer per well, 10 µL of neuraminidase per well, and 0~10 µL of neuraminidase inhibitor samples to be screened per well. After that, 0~10 µL of pure water was added to each hole so that the total volume of each hole was 90 µL. After the inhibitor and neuraminidase were thoroughly mixed, 10 µL of neuraminidase fluorescent substrate was added to each well. Subsequently, fluorescence determination was performed after incubation at 37°C for 30 min. Neuraminidase (NA) inhibition rate = $[1 - (F_s - F_0)/(F_m - F_0)] \times 100\%$. In the formula, F_s is the fluorescence intensity of the sample, F_m is

the fluorescence intensity of the negative control, and F_0 is the fluorescence intensity of the zeroing hole.

Immunofluorescence and immunoblotting analysis

The cells were washed three times with phosphate buffer saline (PBS) before 4% paraformaldehyde fixation (30~60 min). They were then drilled with 0.2% triton X-100. Before incubation with primary antibodies (overnight at 4 °C), the cells were blocked with 2% bovine serum albumin (BSA) for 1 h. They were incubated with secondary antibody after washing. The nucleus was stained with 4',6-diamidino-2-phenylindole (DAPI, 10~20 min). For immunoblotting analysis, cells or tissues were lysed with radio immunoprecipitation assay (RIPA) buffer. The protein concentration was measured by bicinchoninic acid protein quantitative kit. The isolated protein lysates were separated by SDS-PAGE and transferred onto PVDF membranes. This was followed by blocking with 5% skin milk in Tris-buffered saline with Tween-20 (TBST) before incubation with the indicated antibodies 1 h. The membranes were then incubated with a secondary antibody (Protein, CA, USA) for 1 h. The membranes were washed 3 times in TBST, for 5 min each time. Subsequently, the membranes were treated for 2 min with the reagent from an Easysee Western Blot Kit. The results were analyzed by ImageJ software (National Institutes of Health, Bethesda, MD). We conducted three independent cell experiments.

Mice infection and quantitative real-time PCR (qRT-PCR) analysis

BALB / c mice were divided into four different groups, with 13 mice in each group, including control group (Control), virus infection group (Virus), virus+taurolidine treatment group (Virus+taurolidine, i.p.), and virus+oseltamivir treatment group (Virus+oseltamivir, p.o.). Two independent experiments were conducted for each group. Influenza viruses (10-fold mouse median lethal dose, $10 \times \text{mLD}_{50}$) were inoculated intranasally (i.n.) into the mice in the virus-infected group, taurolidine-treated group, and oseltamivir-treated group. Taurolidine (400 mg/kg/d) and oseltamivir (25 mg/kg/d) were administrated twice daily (morning and evening), respectively. The body weight and survival status of the mice were recorded daily for two weeks. The lung index was calculated according to the previous method [19–21]. The treatment of all mice was in accordance with the welfare and ethical guidance for Chinese laboratory animals (GB 14925–2001). The agreement was approved by the Animal Welfare and Ethics Committee of the Institute of the Chinese Academy of Agricultural Sciences (permit number: SCXK-2012-017). For cytokine transcriptome analysis,

total RNA was extracted using Trizol reagent (Invitrogen), and reverse transcription was carried out using ImPromp-II reverse transcriptase (Promega). Semi-quantitative PCR using Ampli Taq polymerase (Applied Biosystems) was performed by including [α - 32 P]-dCTP in the reactions. The IAV-specific primer sets were annealed, and their sequences are listed in Table S1 and Table S2.

Pulmonary pathology and hematoxylin-eosin staining

The mice were euthanatized, and the lung tissues were quickly placed in polyoxymethylene solution (4% PFA) to fix for 24–72 h. After fixation, the tissues were embedded in paraffin and randomly sectioned into 4–8 μ m slices. The slices then were made transparency with xylene and soaked in absolute ethanol for 5–10 min. Finally, the slices were stained with hematoxylin-eosin (H&E), dried, and observed under an optical microscope.

Immunohistochemistry (IHC) assay

The immunohistochemistry (IHC) assay was performed according to the previous method [19]. The pathological severity score of the infected mice was based on the percentage of the inflammation area of each slice collected from each animal, using the following scoring system: 0, no pathological changes; 1, affected area $\leq 10\%$; 2, affected area $< 50\%$ and $> 10\%$; 3, The affected area is $\geq 50\%$. When inflammation, hemorrhage and bronchial epithelial necrosis were observed, the score was increased by one point.

Flow cytometry

Peripheral blood from mice in each group was collected into EDTA-anticoagulation tubes. The blood was mixed with red-blood-cell lysis buffer before centrifugation (3000 rpm, 4 $^{\circ}$ C, 10 min). The cells were then incubated with specific antibodies at low temperature for 2 h without light. The antibodies used included APC conjugated CD3 (152306, biolgend, USA), FITC conjugated CD4 (100510, biolgend, USA), PE conjugated CD8 (100708, biolgend, USA), PE conjugated CD16 (158004, biolgend, USA), FITC conjugated CD49b (108905, biolgend, USA), APC conjugated CD163 (156705, biolgend, USA), and APC conjugated CD11c (117310, biolgend, USA). Subsequently, the analysis was performed using the BECKMAN CytoFLEX flow-meter (BECKMAN COULTER, USA). The results were visualized using CytExpert 2.3 software.

Enzyme-linked immunosorbent assay (ELISA)

For the ELISA assay, serum samples from mice in each group were collected randomly. Cytokines (IL1 β , IL-6, TNF- α , IFN- γ) were then detected using a custom Mouse cytokine 10-plex kit using V-PLEX (K15048D, MSD, USA) according to the manufacturer's instructions. Discovery Workbench software (v4.0, MSD Corporation, USA) was used for data analysis.

Transcription sequencing, blood pressure and ultrasound measurements

Transcription sequencing was performed by MAGIGENE Technology (Shenzhen, China). Sequencing libraries were constructed using the Illumina sequencing platform (Illumina, San Diego, CA). the DESeq method was used to analyze the differential expression of mice in from each group. Kyoto Encyclopedia of Genes and Genomes (KEGG) was used for signaling pathway enrichment analysis. The bubble plots were visualized by the R clusterProfiler package (version 4.0.3). For blood pressure and ultrasound measurements, pulmonary artery blood pressure, including systolic blood pressure (SBP) and diastolic blood pressure (DBP), was measured on days 0, 3, 5, 7, 10 and, 14, respectively. Mean arterial pressure (MAP) was calculated as $MAP = DBP + (1/3 \times SBP)$. In brief, mice were anesthetized before pulse wave velocity (PWV) and pulmonary aorta thickness were measured using an ultrasound instrument (FUJIFILM VisualSonics, Toronto, Canada). Visual image processing was performed using Vevo[®]LAB software.

Ca²⁺ measurement

Cells were treated with or without taurolidine at the designated time after virus-inoculated. For mouse serum samples, serums collected from the blood samples of mice was utilized for subsequent determination. The cell suspension and mouse serum were then harvested for Ca²⁺ determination performed by a kit from Genmed Scientifics Inc. U.S.A (GMS50097.1 v.A). Simply, mixing 100 μ L of the test solution (cell suspension or serum) was mixed with the reaction solution, incubate at room temperature in the dark for 5 min, and the reading was taken using a spectro-photometer. The corresponding Ca²⁺ concentration (mmol/L) of the samples were calculated according to the standard curve. The cultured cells were washed and incubated with the Fluo-4 following AM detection kit (F14202, Invitrogen) before data collection using FDSS/ μ CELL (Hamamatsu Photonics, C13299, Japan). In calcium imaging analysis, the Fluo-4-loaded cells were incubated with the fluorescent probe. Subsequently, calcium imaging was performed using

a fluorescence microscope (LEICA, DMI8, Italy) after the cells were washed with PBS. We conducted three independent cell experiments, with three replicate wells were for each treatment group in each experiment.

Collagen gel-based contraction assay

The contraction of HUVEC cells was evaluated by a collagen gel-based assay according to the method of SakotaY with minor modifications [22]. The cells were suspended in Dulbecco's phosphate buffer solution (DPBS) supplemented with type-I collagen, seeded into a 12-well microplate at a density of 1×10^5 cells/mL, and then incubated for 30 min at 37 °C in a CO₂ incubator for gelation. After adding the culture medium (an equivalent volume to the gel) onto the gel, the embedded cells were cultured for 2 days with the medium being changed daily. The gel was detached from the well using a 10 µl pipette tip, immersed in the assay medium containing the treatment agent, and photographed using a digital camera. Contraction was expressed as the percentage of the gel area relative to that before treatment. Three independent cell experiments were conducted, with three replicate wells set for each treatment group in each experiment.

Hematological analysis

Whole blood from mice in each group was collected in sterile EDTA-anticoagulation tubes. The samples then were analyzed using an automatic hematology analyzer (Mindray Medical, BC-5000, China). Hematological indicators, such as white blood cell counts (WBC), red blood cell counts (RBC), and platelet counts (PLT) were observed and recorded.

Data statistical analysis

Statistical comparisons were performed using Graphpad Prism 8.0 software. A T-test was used to compare the differences between two groups, while ANOVA was performed for comparisons among three or more groups. Quantitative datasets were presented as means ± standard deviation (SD). A *p* values less than 0.05 (*p* < 0.05) was considered statistically significant, with **p* < 0.05, ***p* < 0.01, and ****p* < 0.001 indicating different levels of significance.

Results

Administration of taurolidine inhibited the reproduction of influenza virus in vitro

The potential anti-influenza virus activity of taurolidine was evaluated using an MDCK cell infection model. Taurolidine efficiently inhibited IAV/H1N1 replication in cultures exposed to different dose-ranges of the drugs for 24 h (Fig. 1A, left). The 50% effective concentration (EC₅₀ value) of taurolidine was determined to be 31.63 µg/mL (Fig. 1B, left). Similarly, we found that taurolidine inhibited IBV/S9-MD replication as well (Fig. 1A, right), with an EC₅₀ value of 22.73 µg/mL (Fig. 1B, right). To rule out the possibility that the reduction in viral replication was an indirect effect on host cell, MTT experiment was performed to assess the cytotoxicity of taurolidine. The results showed that taurolidine did not significantly reduce the viability of MDCK cells (Fig. S1A) and A549 cells (Fig. S1B) at concentrations of 10, 25, 50 and 100 µg/mL. This suggests that taurolidine mainly exerts its antiviral effect by directly inhibiting the proliferation of influenza viruses. The antiviral activity of taurolidine against influenza virus was further confirmed using plaque reduction assays. As shown in Fig. 1C, plaque formation in IAV/H1N1- and IBV/S9-MD-infected cells was significantly reduced after treatment with taurolidine.

To explore the potential antiviral effects of taurolidine, oseltamivir (a common anti-influenza drug) was used as a positive control in an indirect immunofluorescence assay. As anticipated, oseltamivir significantly inhibited the propagation of the IAV/H1N1 strain. In DMEM-treated cells, 38% of MDCK cell nuclei were virus NP-positive for the virus, whereas taurolidine treatment significantly reduced the percentage of NP-positive cells to 9.8% (Fig. 1D). Comparable results were observed for the IAV/H1N1 and IBV/S9-MD strain (Fig. 1E). The hemagglutination (HA) test further showed that taurolidine exhibited strong antiviral activity (Fig. S1C, D). In addition, the protein expression level of virus NP was significantly decreased after taurolidine treatment in both IAV/H1N1-infected and IBV/S9-MD-infected cells (Fig. 1F).

To clarify the active stage of taurolidine against the influenza virus, we treated A549 cells using three different infection protocols, including pre-treatment, co-treatment and post-treatment (Fig. S1E). It was observed that post-treatment with taurolidine exhibited high inhibition rates in IAV/H1N1-infected (Fig. 2A), IAV/H3N2-infected (Fig. 2B), and IBV/S9-MD-infected cells (Fig. 2C), indicating that taurolidine inhibits later stages of influenza virus infection. To further assess the antiviral potential of taurolidine, different influenza virus subtypes (IAV/H1N1-PR8,

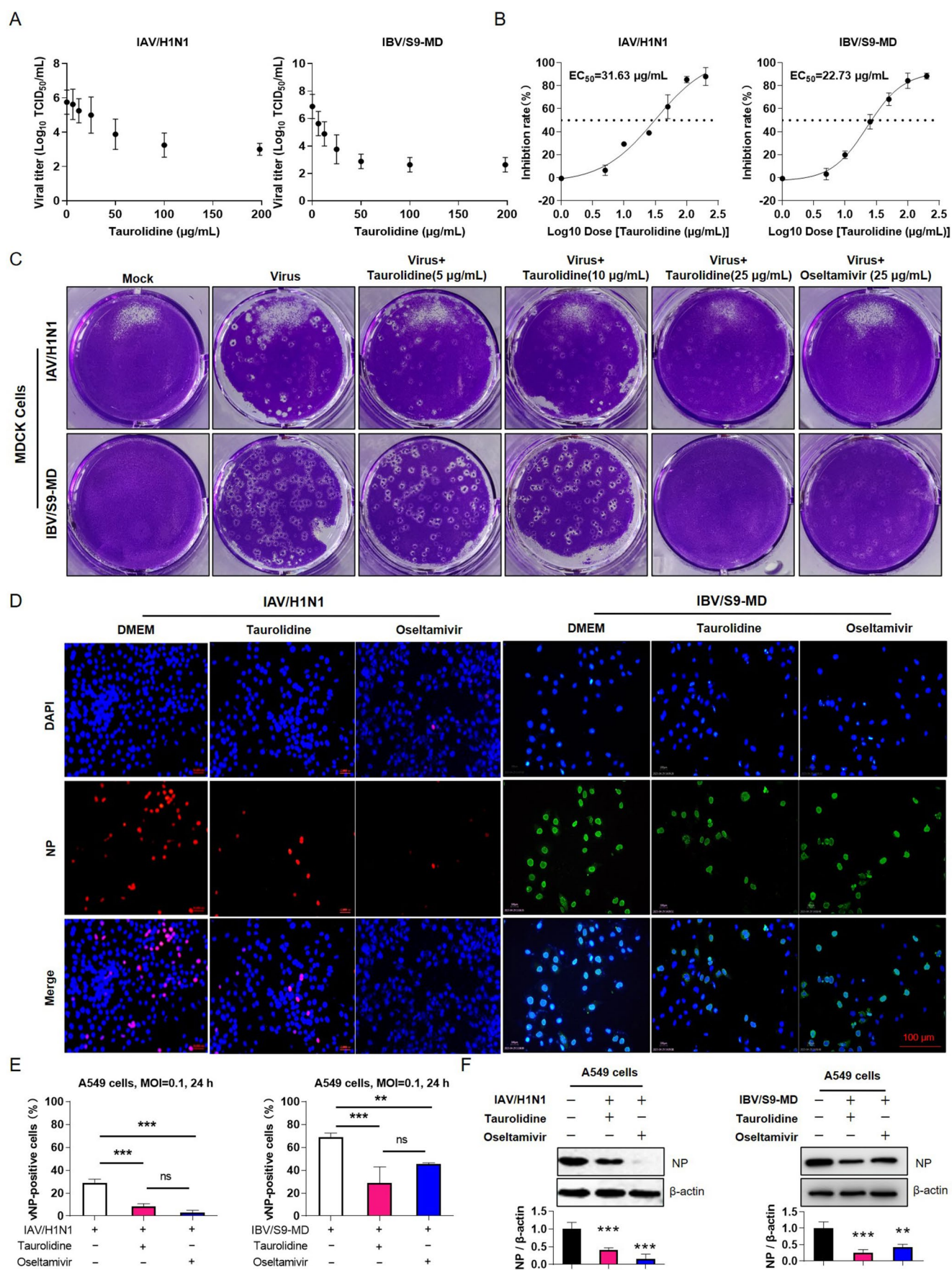


Fig. 1 Taurolidine inhibits the reproduction of influenza virus in vitro. (A) Dose-response curve of taurolidine against viral titers in MDCK cells infected with IAV/H1N1 and IBV/S9-MD. (B) The semi-logarithmic fitting curve was plotted by converting the concentration of taurolidine into a logarithmic scale and the virus titer into percentage, and the EC_{50} value was calculated from this curve. (C) Plaque assay in MDCK cells infected with IAV/H1N1 and IBV/S9-MD. The experiment was performed independently in triplicate with duplicate plaque assays, and representative pictures are shown. (D) Immunofluorescence against viral nucleoprotein (virus NP), the scale bar set to 10 μ m. A549 cells were infected with influenza virus at an MOI of 0.1, followed by treatment with DMEM (solvent) and taurolidine (50 μ g/mL) for 24 h. OSTA (50 μ g/mL) was used as a positive control. The nucleus was stained with DAPI, and infected cells were detected by nuclear staining for viral NP (scale bar 10 μ m). (E) The percentage of virus NP-positive cells in Fig. 1D was calculated. (F) Western blotting experimental results of virus NP in A549 cells infected with IAV/H1N1 and IBV/S9-MD, using β -actin as a loading control

IAV/H1N1-UI182, IAV/H3N2 and IBV/S9-MD strains) were chosen to infect A549 (Fig. 2D, E, F, G) and MDCK cells (Fig. 2H, I, J, K), respectively. Considering the virus neuraminidase (NA) activity is required for the release of virions, we subsequently examined the NA activity. The results found that taurolidine inhibited the NA activity in a dose-dependent manner (Fig. 2L, M, N, O), which indicating that taurolidine had an inhibitory effect on later stages of influenza virus. These results indicate that taurolidine showed significant inhibitory activity against various subtypes of the influenza virus.

Taurolidine improves the survival rate after influenza virus infection

The therapeutic effect of taurolidine was further evaluated in mouse models due to its obvious anti-influenza activity observed in vitro. We found that taurolidine treatment alleviated weight loss in mice infected with influenza viruses, including IAV/H1N1 (Fig. 3A), IAV/H3N2 (Fig. 3B), and IBV/S9-MD (Fig. 3C). Compared to virus-infected mice, taurolidine treatment significantly improved the overall survival of mice in the drug-treatment groups, with protection rate of 66.67% for IAV/H1N1 (Fig. 3D), 42.86% for IAV/H3N2 (Fig. 3E), and 66.67% for IBV/S9-MD (Fig. 3F). Subsequently, we examined the viral loads in the lung tissues of mice at 3 dpi and 5 dpi, and found that viral loads were significantly reduced in the taurolidine-treated groups (Fig. 3G, H, I). Furthermore, western blot results confirmed that taurolidine significantly inhibited the replication of influenza viruses in the mice lung tissues (Fig. 3J, K, L). By observing the lung morphology, we found that both IAV/H1N1 and IBV/S9-MD infection caused extensive bleeding (**black arrow**) in the lung tissue of mice, while taurolidine significantly reversed these results (Fig. 4A). The lung index of mice infected with IAV/H1N1 (Fig. 4B) and IBV/S9-MD (Fig. 4C) also decreased after taurolidine treatment.

To investigate the effect of taurolidine on lung pathology caused by influenza virus infection, lung tissues were randomly collected from mice in each group at 5 dpi for H&E and IHC assays. The H&E assay showed that influenza virus infection caused cell necrosis (**red arrow**) and inflammatory cell infiltration (**blue arrow**), but these effects were inhibited by the administration of taurolidine (Fig. 4D). Furthermore, the pathological score confirmed that taurolidine treatment improved overall lung pathology in mice infected with influenza virus (Fig. 4E, F). In addition, we found that taurolidine administration significantly inhibited the expression of virus NP in lung tissues (Fig. 4G), and reduced the number of NP-positive cells in the lung tissues of mice infected with IAV/H1N1 (Fig. 4H) and IBV/S9-MD (Fig. 4I). Moreover, we observed that taurolidine treatment significantly increased the number of white blood cells (Fig. S2A, B), reduced the number of red blood cells (Fig. S2C), and reduced the number of the number of platelets in mice infected with IAV/H1N1 (Fig. S2D). Similar results were observed in mice infected with IBV/S9-MD (Fig. S3). These results indicated that taurolidine treatment effectively mitigates the pathological damage caused by influenza viruses and improves the survival rate of infected mice.

Effects of taurolidine on immune cell and cytokine storm induced by influenza virus infection

We previously demonstrated that taurolidine treatment improved inflammatory cell infiltration caused by influenza virus infection in the lung tissues of infected mice. To further analyze the effects of taurolidine on immune cells in influenza virus-infected mice, peripheral blood was collected from mice in each group at 5 dpi for flow cytometry analysis. The results showed that influenza (IAV/H1N1) virus infection led to a reduction in the ratio of $CD4^+$ T cells (Fig. S4A) and $CD8^+$ T cells (Fig. S4B), and the administration of taurolidine reversed this effect (Fig. S4B; Fig. S4B). Interestingly, we observed a reduction in $CD8^+$ T cells (Fig. S4C) but no significant changes in $CD4^+$ T cells in IBV/S9-MD-infected mice (Fig. S4C, D). Importantly, taurolidine treatment also improved the $CD8^+$ T cells reduction caused by IBV/S9-MD infection (Fig. S4D). In addition, we found that influenza (IAV/H1N1) virus infection increased the ratio of neutrophils, macrophages, natural killer (NK) cells, and dendritic cells (Fig. S4E). However, the results of quantitative analysis showed that taurolidine treatment significantly reduced the number of neutrophils (Fig. S4F), macrophages (Fig. S4G), NK cells (Fig. S4H), and dendritic cells (Fig. S4I). These findings suggest that taurolidine treatment reduces the ratio of immune cell caused by influenza virus infection.

Inflammatory cytokines are markedly elevated after influenza virus infection, and the cytokine storm is considered

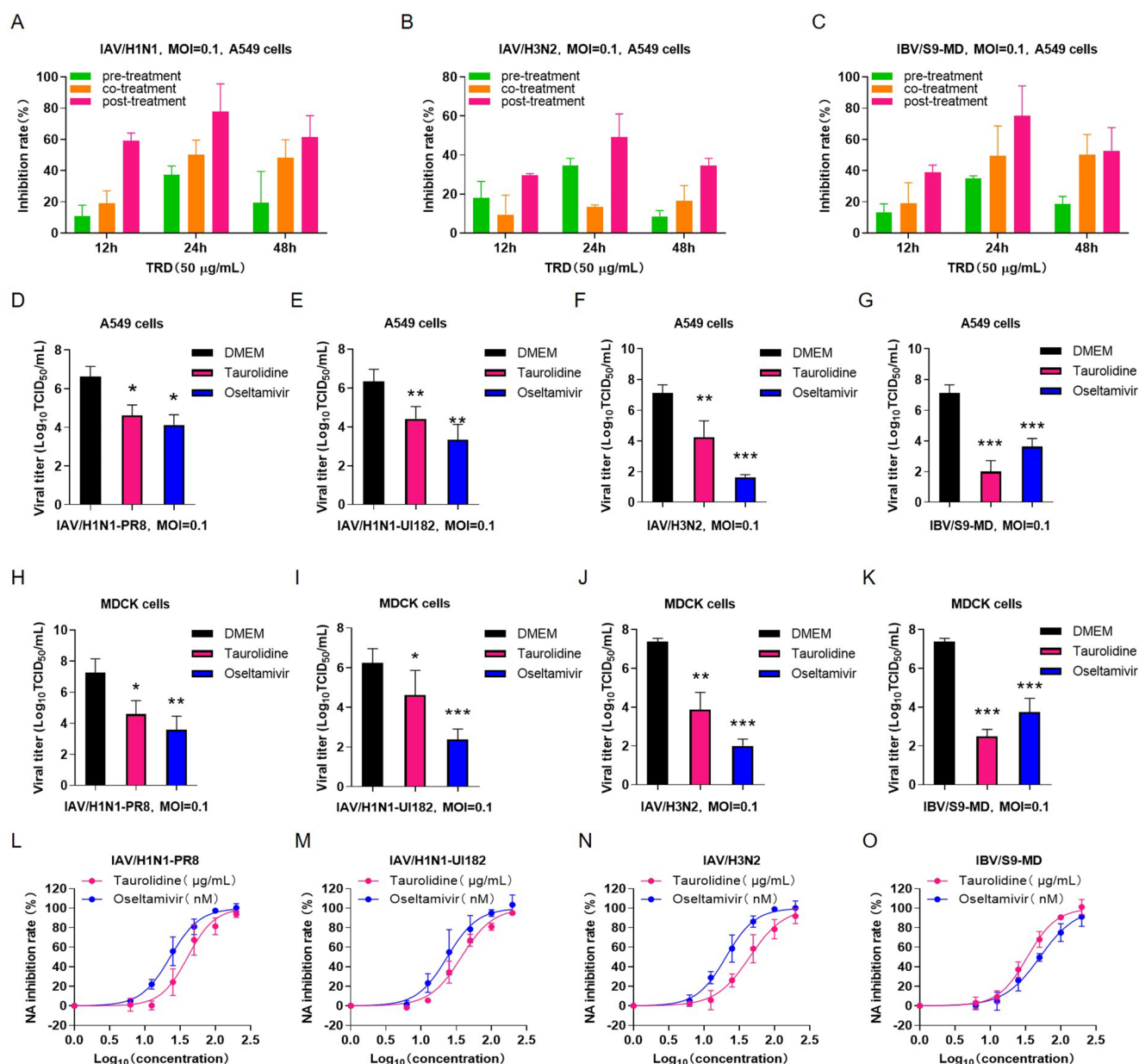


Fig. 2 Taurolidine antiviral activity is not specific to virus subtypes or cell lines. **(A–C)** The inhibitory rates of taurolidine against influenza viruses with different infection protocols were evaluated in A549 cells, including IAV/H1N1, IAV/H3N2, and IBV/S9-MD. **(D–G)** After infecting A549 cells with influenza viruses (IAV/H1N1-PR8, IAV/H1N1-UI182, IAV/H3N2, and IBV/S9-MD) at an MOI of 0.1, the cells were treated with DMEM and taurolidine (50 µg/mL) for 24 h. Oseltamivir (OSTA, 50 µg/mL) was used as a positive control, and

the virus titer was determined in MDCK cells. **(H–K)** After infecting MDCK cells with influenza viruses (IAV/H1N1-PR8, IAV/H1N1-UI182, IAV/H3N2, and IBV/S9-MD) at an MOI of 0.1, the cells were treated with DMEM and taurolidine (50 µg/mL) for 24 h. Oseltamivir (OSTA, 50 µg/mL) was used as a positive control, and the virus titer was determined in MDCK cells. **(L–O)** The NA activity was detected in A549 cells infected with influenza virus

the main cause of mortality. To investigate the effect of taurolidine on the inflammatory response induced by influenza (IAV/H1N1) virus infection, we collected the serum from each group of mice for ELISA detection. The results showed that taurolidine reduced the concentration of key inflammatory cytokines in the serum, such as IL-6 (Fig. 5J), IFN-γ (Fig. 5K), TNF-α (Fig. 5L), and IL-1β (Fig. 5M).

In addition, we observed that influenza (IAV/H1N1) virus infection leads to up-regulation of cytokine mRNA expression in the lungs of infected mice. Taurolidine treatment significantly reduced the mRNA expression of cytokines and chemokines, including *CCL2*, *CCL3*, *CCL5*, *CXCL10*, *CXCL11*, and *IFN-α*, *IFN-γ*, as well as *IL-6*, *IL-10*, *IL-1β*, and *TNF-α* (Fig. S5). These findings suggest that taurolidine

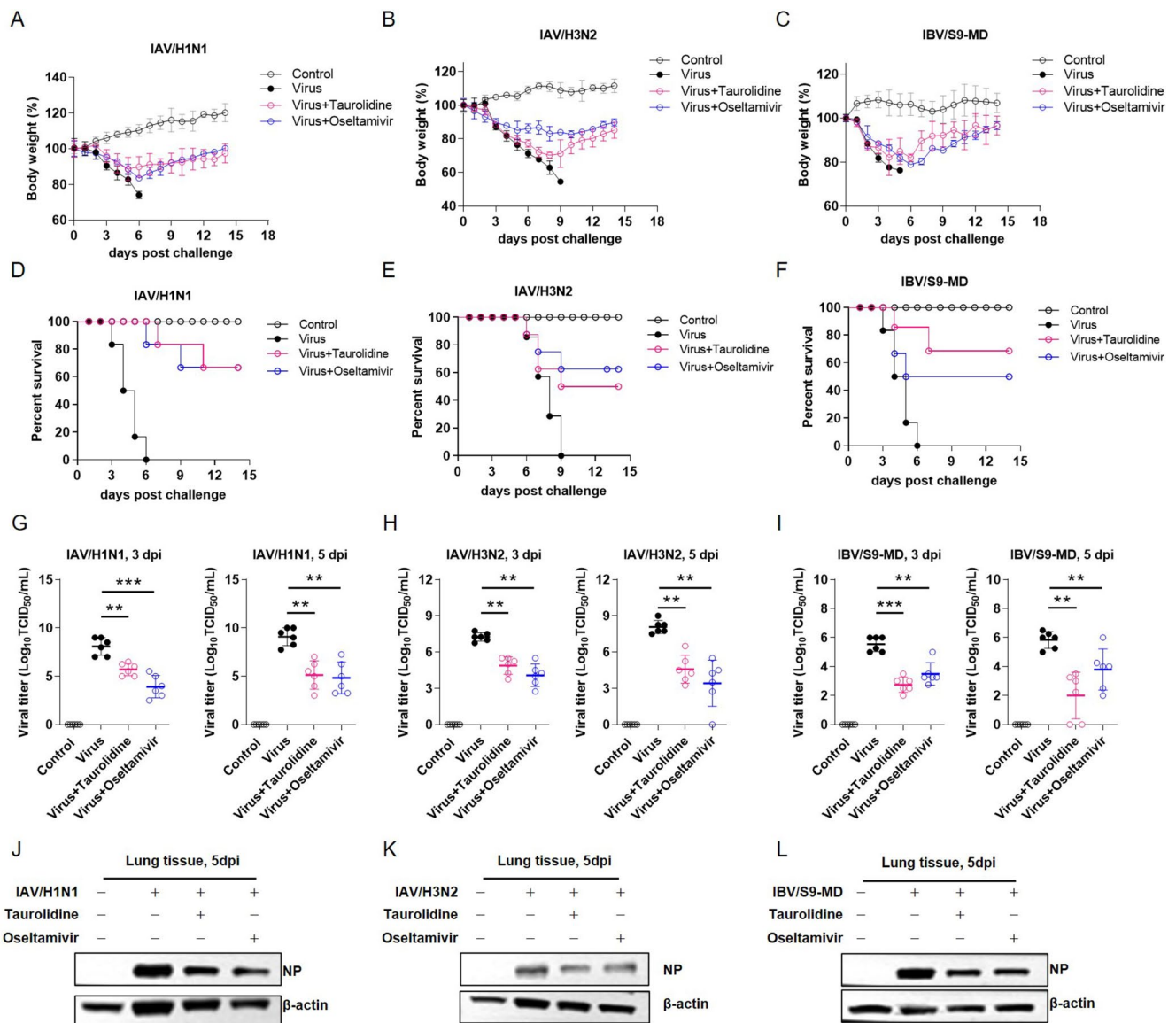


Fig. 3 The antiviral effect of taurolidine against influenza viruses in mouse model. (**A–C**) Body weight changes in the control group (Control, gray), virus group (Virus, black), taurolidine treatment group (Virus+taurolidine, purple), and oseltamivir treatment group (Virus+oseltamivir, blue), including IAV/H1N1, IAV/H3N2, and IBV/S9-MD. (**D–F**) Survival rate of infected mice treated or untreated with taurolidine. (**G–I**) Virus titer in mouse lung tissues at 3- and 5-day post infection (dpi). (**J–L**) The protein expression level of influenza virus NP in the lung tissues of mice at 5 dpi was analyzed by Western blot, using β-actin as a loading control

reduces the expression of cytokines and chemokines in mouse lungs following influenza virus infection.

Taurolidine alleviates vascular pathology in mice infected with influenza virus

As a fast-track mechanism for immune regulation, blood vessels regulate the transportation and transfer of immune cells during influenza virus infection. In this study, we sought to investigate the effects of taurolidine treatment on blood pressure in mice infected with the influenza virus. The results showed that systolic blood pressure (SBP), diastolic

blood pressure (DBP), and mean arterial pressure (MAP) were significantly increased in mice infected with influenza virus, while taurolidine treatment led to a decrease in these values (Fig. 6A, B, C). Two-dimensional ultrasound results showed that influenza virus infection caused thickening of the pulmonary aortic wall in IAV/H1N1-infected mice, an effect that was alleviated by taurolidine treatment (Fig. 6D). Compared to the control group, the pulse wave velocity (PWV) of the pulmonary aorta in IAV/H1N1-infected mice was increased at 5 dpi (3.88 ± 0.38 mm/s vs. 2.02 ± 0.18 mm/s), but this was mitigated following taurolidine treatment (2.86 ± 0.28 mm/s vs. 3.88 ± 0.38 mm/s,

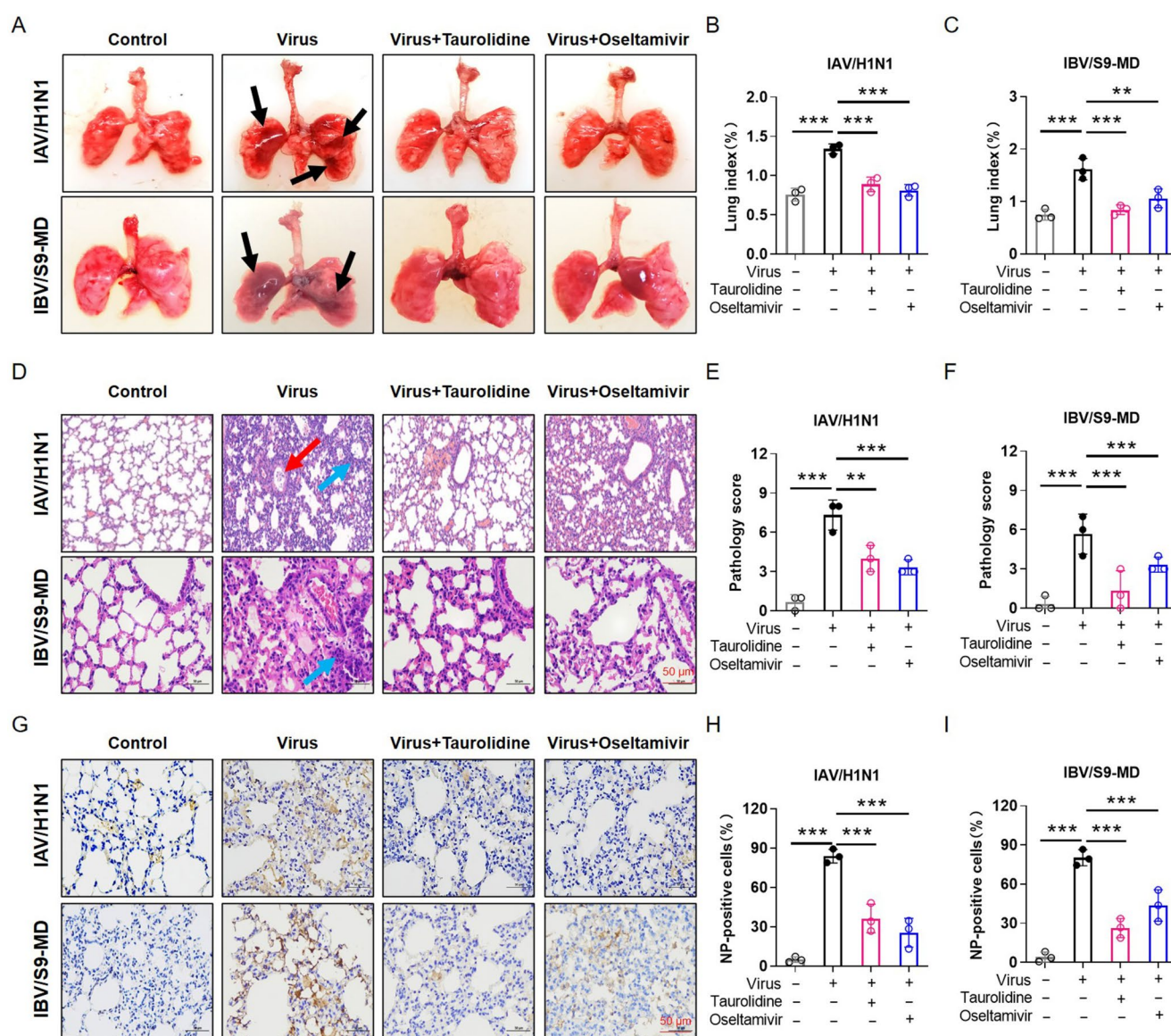


Fig. 4 Taurolidine alleviates the pathogenic effect of influenza virus infection. **(A)** Morphological observation of mice at 5 dpi with IAV/H1N1 and IBV/S9-MD, with bleeding regions indicated by black arrows. **(B, C)** The effect of taurolidine on the lung index of mice was measured at 5 dpi following IAV/H1N1 and IBV/S9-MD infection. **(D)** Hematoxylin-eosin staining of lung tissues from mice in each group, with representative images shown here. The scale bar is 50 μ m.

Green arrows indicate massive lymphocyte infiltration, and red arrows indicate cell debris. **(E, F)** Lung pathology score at 5 dpi. The pathology scores are summarized according to (one point for each of hemorrhage, alveolar wall thickening, inflammation, and cell necrosis), with $n=3$. **(G)** Immunohistochemical analysis of virus NP expression in lung tissues after influenza virus infection. **(H, I)** Quantification of the number of NP-positive cells

Fig. 6E). Moreover, the pulmonary aorta in IAV/H1N1-infected mice exhibited greater thickness and a smaller diameter compared to controls, with these differences being reversed following taurolidine treatment (Fig. 6F, G). Changes in the thickness of the pulmonary aorta were also confirmed by H&E staining (Fig. 6H), and similar results were found in mice infected with IBV/S9-MD (Fig. S6).

Taurolidine inhibits vasoconstriction pathways and intracellular calcium elevation induced by influenza virus infection

We previously shown that taurolidine mitigated vascular changes in the pulmonary artery blood vessels induced by influenza virus infection in mice. To further investigate the effect of taurolidine on the pulmonary artery induced by influenza virus infection, we collected lung tissues from each group of mice to perform transcriptome analysis. The

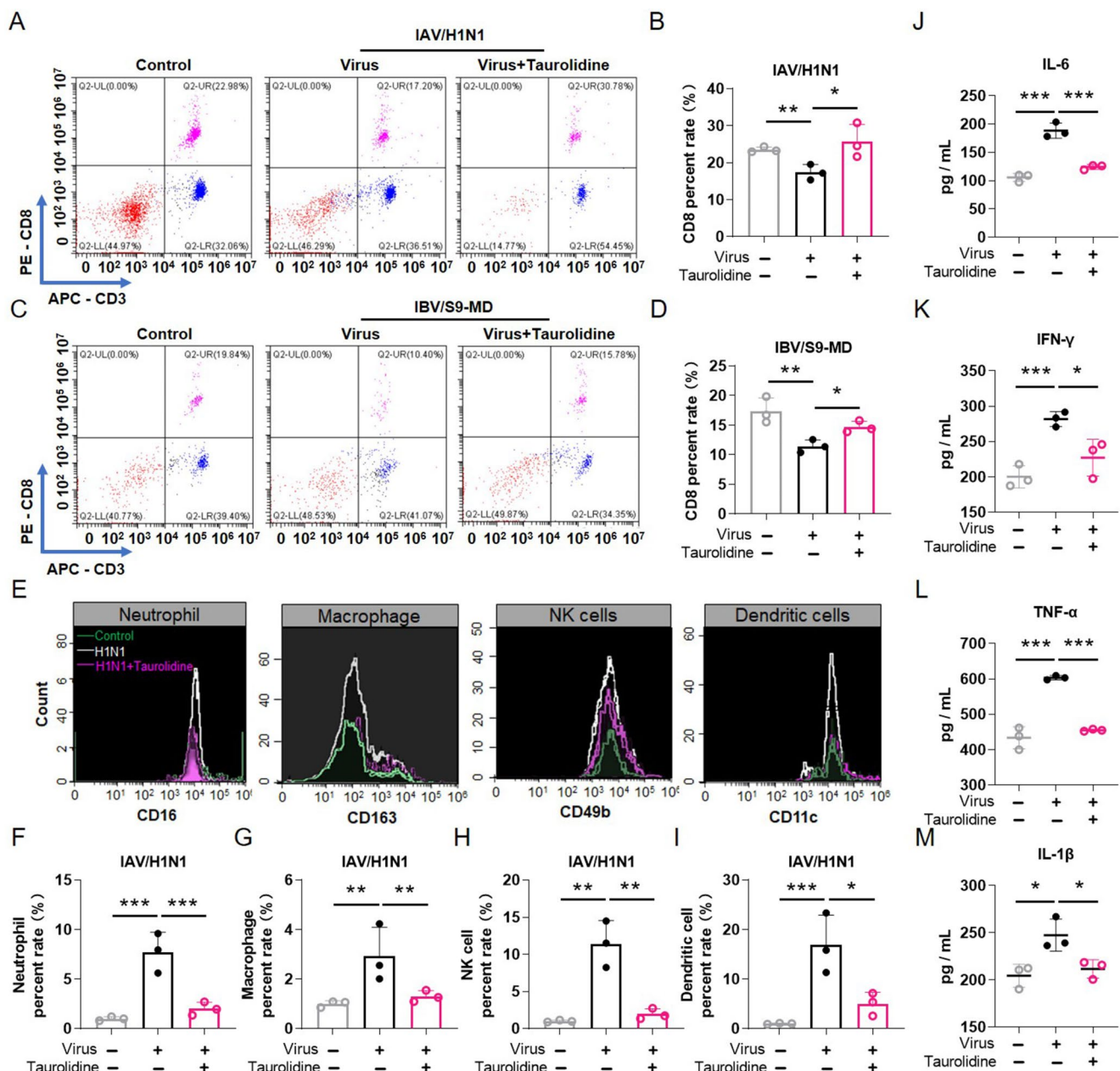


Fig. 5 Effects of taurolidine on immune cell and cytokine storm induced by influenza virus infection. (A) CD8⁺ T cell amount changes in IAV/H1N1-infected mice. (B) Quantification of CD8⁺ T cells seen in Fig. 5A. (C) CD8⁺ T cell amount changes in IBV/S9-MD-infected mice. (D) Quantification of CD8⁺ T cells seen in Fig. 5C. (E) The immune cells change in IAV/H1N1-infected mice, including neutro-

phil, macrophage, NK cell, and dendritic cell. (F) Quantification of neutrophil seen in Fig. 5E. (G) Quantification of macrophage seen in Fig. 5E. (G) Quantification of NK cell seen in Fig. 5E. (G) Quantification of dendritic cell seen in Fig. 5E. (J-M) Levels of proinflammatory cytokines were analyzed in serum of IAV/H1N1-infected mice at 5 dpi by ELISA

results showed that the vascular smooth muscle contraction signaling pathway was significantly enriched after infection with influenza viruses IAV/H1N1 (Fig. 7A) and IBV/S9-MD (Fig. 7B). Subsequently, the expressions of some genes in the vascular smooth muscle contraction signaling pathway were detected. Taurolidine treatment rescued the down-regulation of *PKC*, *ADER5*, *MYLK3*, *PPP1C* and

MLC1 expression in lung tissues of mice infected with IAV/H1N1 (Fig. 7C) and IBV/S9-MD (Fig. 7D).

Generally, the contraction and relaxation of vascular smooth muscle mainly depend on the state of membrane light chain (MLC) phosphorylation, which is regulated by Ca²⁺/calmodulin complex, as well as by MLC kinase and MLC phosphatase [23, 24]. Thus, we examined the concentration of Ca²⁺ in VSMCs after influenza virus infection. We found

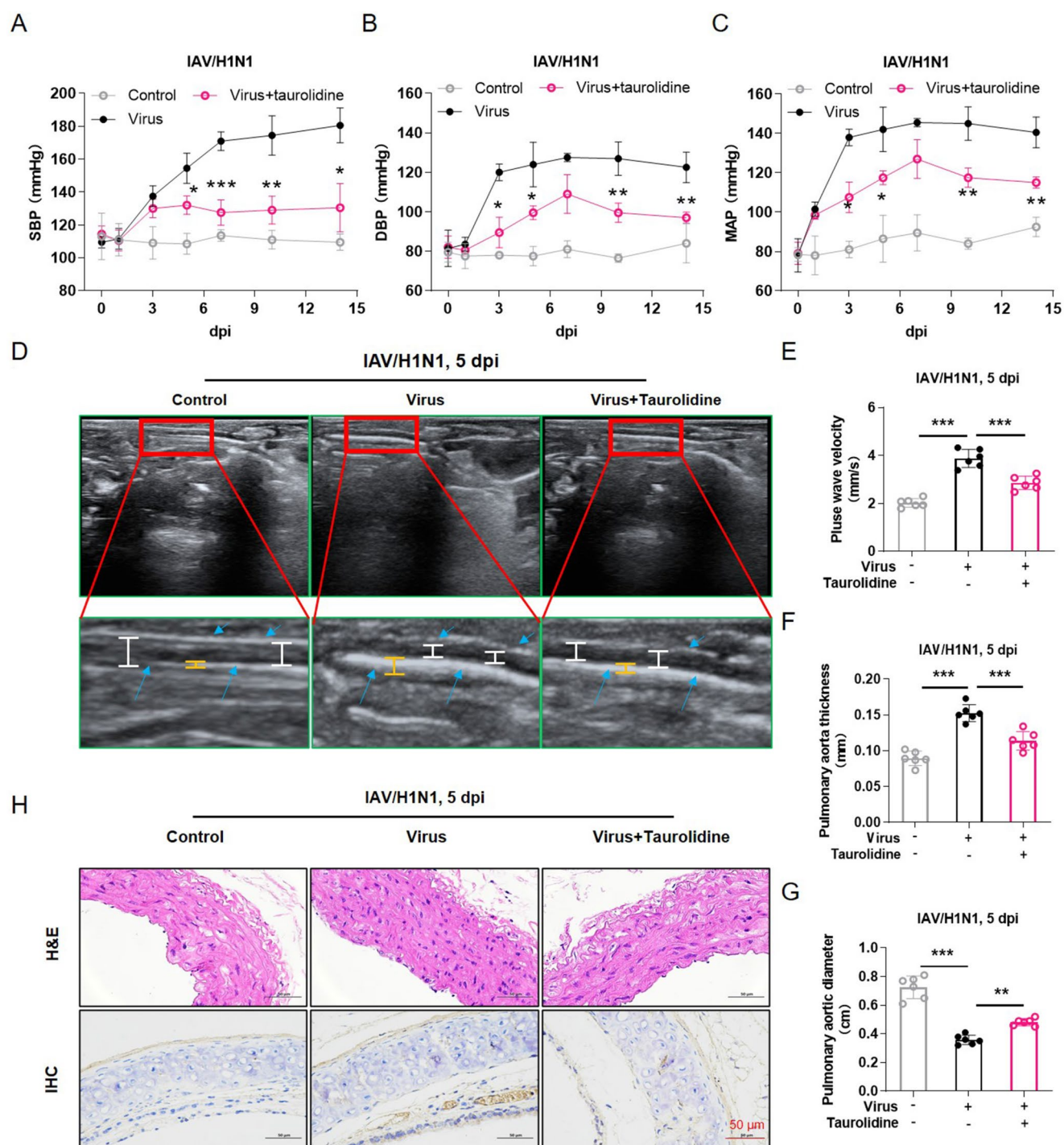


Fig. 6 Taurolidine alleviates vascular pathology in mice infected with influenza virus. The blood pressure of IAV/H1N1-infected mice were measured, including (A) systolic blood pressure, (B) diastolic blood pressure and (C) mean arterial pressure. (D) Ultrasound assay was used to measure the pulmonary aorta of IAV/H1N1-infected mice at 5 dpi, and the representative ultrasonography images of the pulmonary aorta are shown. (E) Pulse wave velocity of the pulmonary aortic

measured by ultrasound. (F) Thickening of the pulmonary aortic wall measured by ultrasound. (G) The pulmonary aortic diameter of the pulmonary aortic wall measured. (H) Representative cross-sections of pulmonary aortic tissues stained with H&E, and Immunohistochemical analysis of virus NP expression intensity in the pulmonary aortic of IAV/H1N1-infected mice

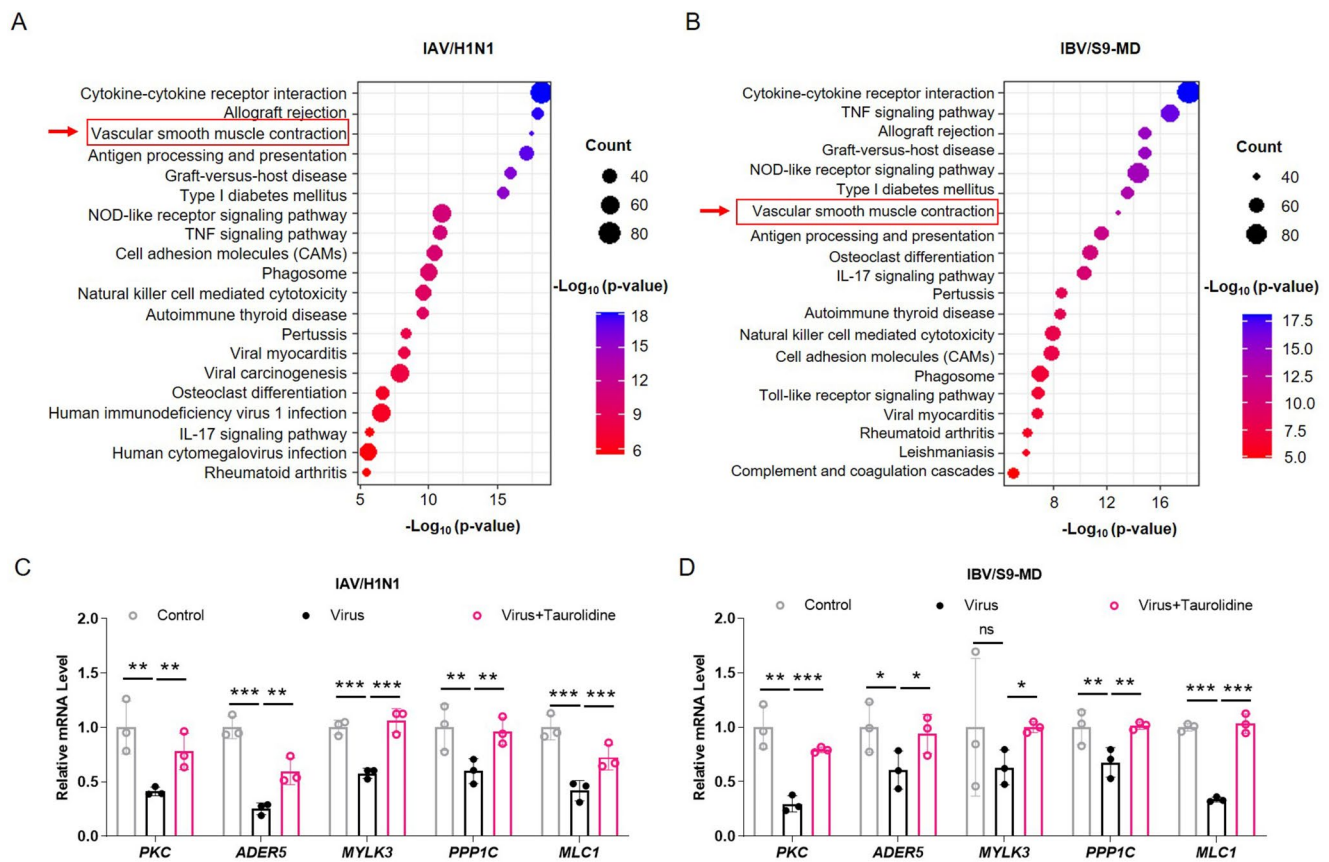


Fig. 7 Taurolidine inhibits vasoconstriction pathways activated by influenza virus infection. (**A**, **B**) KEGG pathway enrichment analysis of differentially expressed transcripts (DETs) comparing the virus

and virus + taurolidine groups. (**C**, **D**) The mRNA expression levels of genes related to vascular smooth muscle contraction signaling

that both IAV/H1N1 and IBV/S9-MD infection increased in intracellular Ca^{2+} concentration, which was subsequently attenuated by taurolidine treatment in a time-dependent manner (Fig. 8A, B). By comparing the intracellular Ca^{2+} signaling intensity, we also found that taurolidine treatment reduced Ca^{2+} concentration in a dose-dependent manner after IAV/H1N1 infection (Fig. 8C, D, E, F). In addition, taurolidine-treated significantly decreased the phosphorylated expression level of MLC (p-MLC) and increased the protein expression level of MLC in a dose-dependent manner in VSMCs infected with IAV/H1N1 (Fig. 8G) or IBV/S9-MD (Fig. 8H), which was not observed after oseltamivir treatment (Fig. S7A, B). The collagen gel-based contraction assay also found that taurolidine treatment increased the initial area of IAV/H1N1-infected VSMCs compared to the untreated group (Fig. S8A, B), suggesting that taurolidine controls vascular smooth muscle contraction after influenza virus infection.

Taurolidine attenuates the activation of MLCK/p-MLC pathway induced by influenza virus infection

We previously shown that the phosphorylated expression level of MLC (p-MLC) was down-regulated and the protein expression level of MLC was up-regulated in VSMCs after infection with influenza (IAV/H1N1) virus (Fig. 8G), while it was attenuated by taurolidine treatment in a dose-dependent manner (Fig. S9). To investigate taurolidine regulation in vasoconstriction signaling pathway induced by influenza virus infection, western blot was performed. The results showed that influenza (IAV/H1N1) virus infection up-regulated the protein expression levels of AT1R (Fig. 9A), CaM (Fig. 9B), and MLCK (Fig. 9C), but this was reversed by taurolidine treatment in a dose-dependent manner. Considering the stability of the in vitro environment, we subsequently focused on in vivo experiments. In immunohistochemical (IHC) staining of the pulmonary aorta of mice infected with influenza virus, significant up-regulation of p-MLC was observed in the pulmonary aorta of IAV/H1N1-infected mice, and it was reversed by taurolidine treatment (Fig. 9D). Similarly, IAV/H1N1 infection

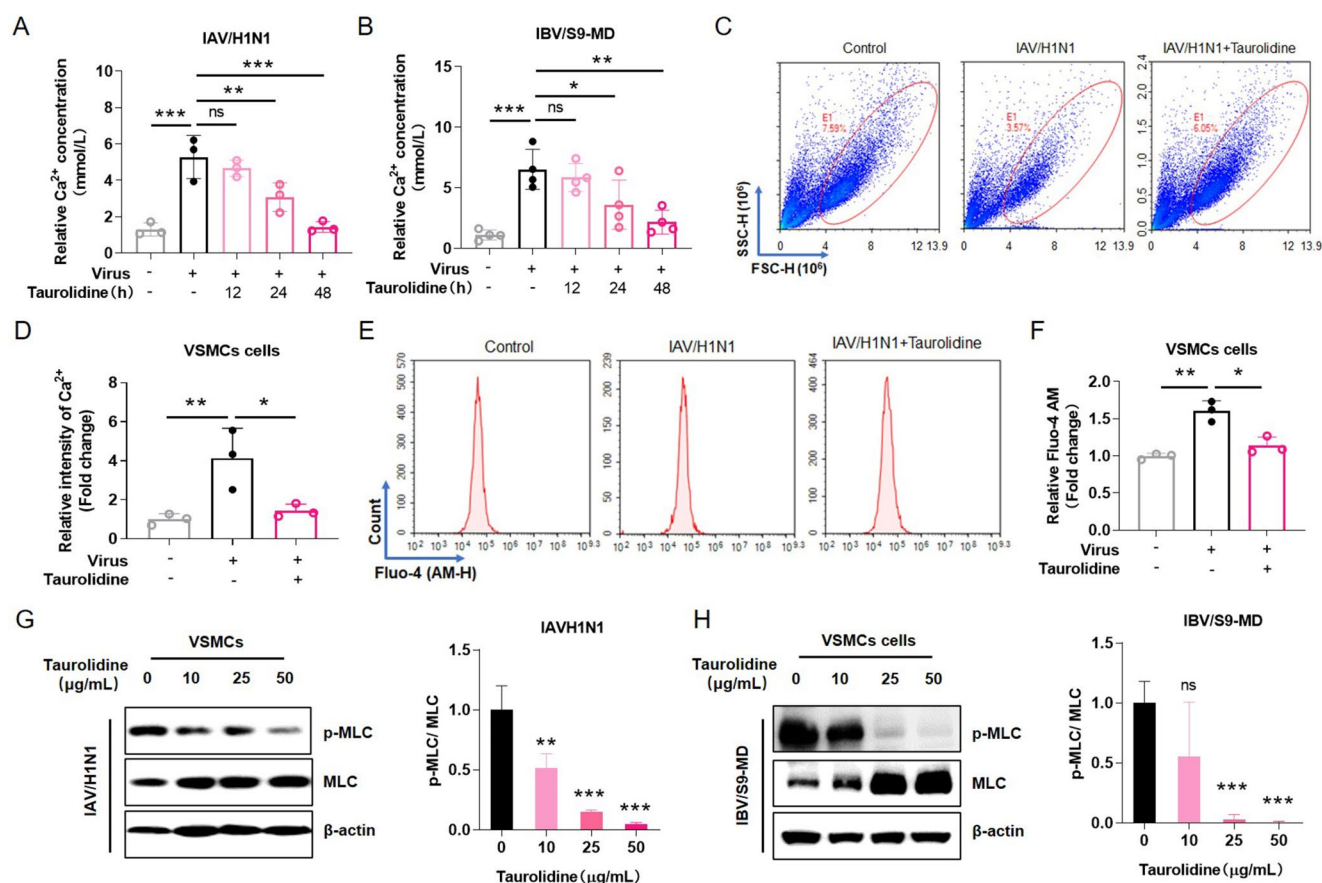


Fig. 8 Taurolidine inhibits intracellular calcium release by influenza virus infection. (**A**, **B**) The intracellular Ca^{2+} concentration was measured after VSMCs cells were infected IAV/H1N1 and IBV/S9-MD, respectively. (**C**) The Ca^{2+} intensity in IAV/H1N1-infected VSMCs (with or without drug treatment) was measured. (**D**) Quantitative analysis of the relative calcium intensity of each group as in **C**. (**E**)

The Ca^{2+} signaling in IAV/H1N1-infected VSMCs (with or without drug treatment) was measured. (**F**) Quantitative analysis of the relative calcium intensity of each group as in **E**. (**G**) Western blotting results of p-MLC and MLC in VSMCs after IAV/H1N1 infection. (**H**) Western blotting results of p-MLC and MLC in VSMCs after IBV/S9-MD infection

also down-regulated the protein expression level of MLC and up-regulated the protein expression level of AT1R, CaM, and MLCK in the pulmonary aorta of IAV-infected mice (Fig. 9E), all of which were reversed by taurolidine treatment.

Discussion

The continuous replication, recombination and mutation of influenza virus have presented significant challenges for the prevention and treatment of influenza diseases [25]. Current antiviral countermeasures primarily consist of preventive vaccines and therapeutic drugs. Despite partial achievements have been obtained, but resistance to existing antiviral drugs has become a serious problem [26]. Thus, repurposed of old drugs is also a selection strategy in combating the virus due to their low-toxicity and high-efficiency in clinical application. In this study, we found

that the clinically licensed antibacterial drug taurolidine significantly inhibited the replication of influenza viruses in vitro and improved the survival rate of lethal influenza virus infection in mouse models by suppressing cytokine storms and regulating vasoconstriction.

As a derivative of taurine, taurolidine has been proved to be an effective antibacterial agent and used to therapy peritonitis in some countries. Previous studies have shown that it inhibits the synthesis of IL and TNF in human peripheral blood mononuclear cells [18], which indicates that taurolidine is likely to play important roles in IL- and TNF-induced related diseases. Indeed, the application of taurolidine tends to prevent the development of lung metastases [27]. In our study, we found that taurolidine significantly improved the lung damage caused by influenza virus infection in mice. Moreover, the drug treatment significantly reduced the number of neutrophils after influenza virus infection. However, the detailed mechanism behind this requires further studied in future.

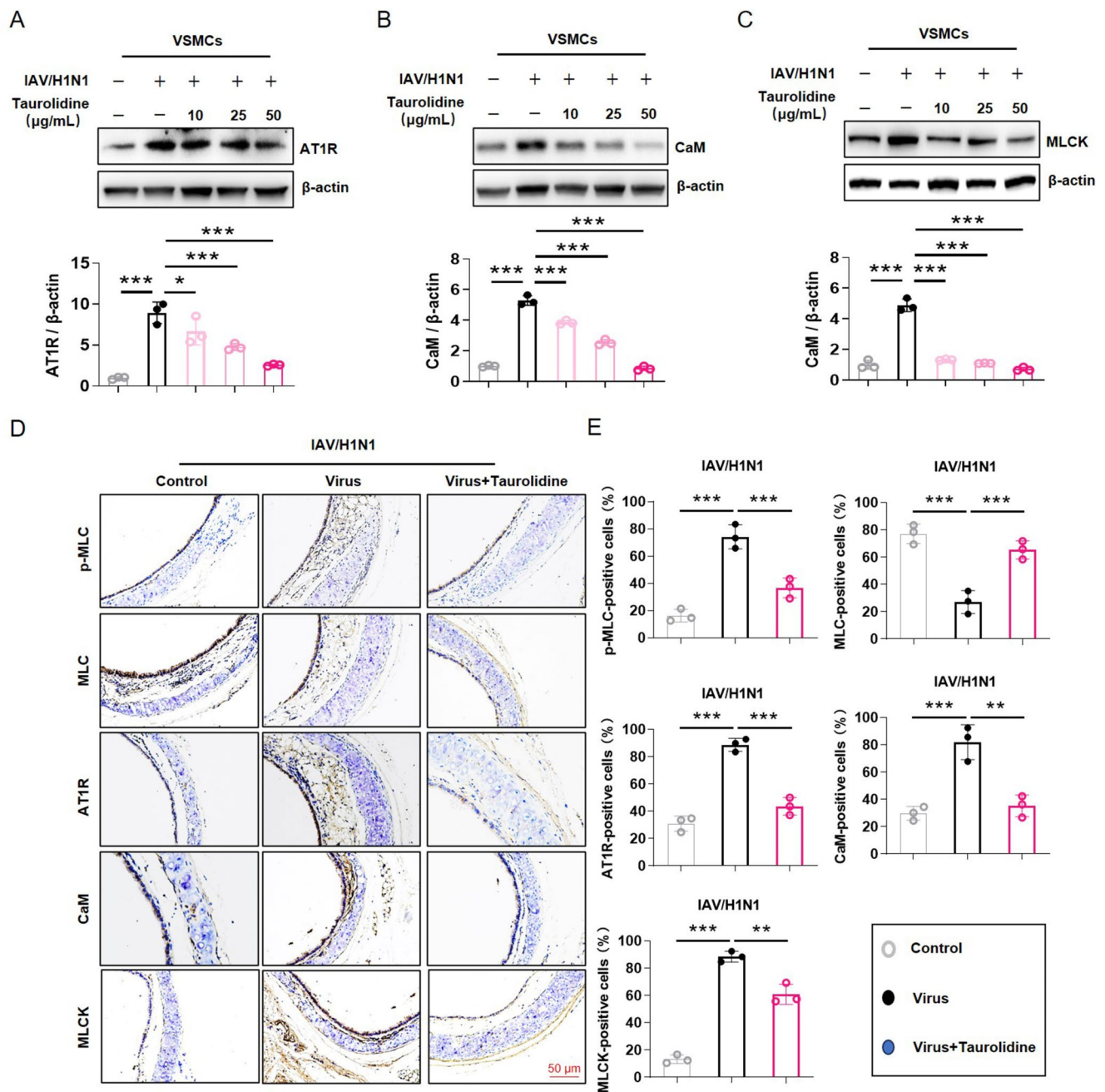


Fig. 9 The effects of taurolidine on the MLCK/p-MLC pathway induced by influenza virus infection. Western blotting was used to determine protein levels of (A) AT1R, (B) CaM and (C) MLCK in IAV/H1N1-infected VSMCs post-treated with taurolidine (10, 25,

50 μ M) for 24 h. (D) Immunohistochemical staining was used to detect protein levels of p-MLC, MLC, AT1R, CaM and MLCK in pulmonary aorta tissues. (E) Quantification of the number of positive cells for p-MLC, MLC, AT1R, CaM, and MLCK

The clinical outcome after virus infection depended largely on the balance between virus replication and host defense response [28]. The ability of the virus to evade the host's immune response is critical to its pathogenicity [29]. Overexpression of inflammatory factors in the host after influenza virus infection will lead to death, and this effect can be improved by inhibition of cytokine regulating inflammation molecular information [30]. Additionally, cytokines

play important roles in activating immune cells, regulating immune responses, and promoting virus clearance, which suggest that their dynamic balance usually determines the process of host infection [31]. The imbalance of cytokine effect and immune cells recruitment could be used as poor prognostic indicators during highly pathogenic influenza virus infection [32]. Early induction of cytokines (IFN- α , IL-1 β , IL-2, IL-6, and TNF- α) and chemokines (CCL2,

CCL3, CXCL2, and CXCL10) are related to the symptom's formation in human [33, 34]. TNF- α , IL-1, and IL-6 have multifunctional activities and are related to the morbidity after influenza virus infection [35]. In this study, we found that the protein levels of the cytokines (TNF- α , IL-6, and IL-10) in the serum were reduced after influenza virus infection. Additionally, chemokines play a crucial role in recruiting innate immune cells to lung tissues, releasing more cytokines, further exacerbating the cytokine storm [36]. Importantly, we demonstrate that taurolidine significantly reduces the mortality of mice infected with human pathogenic influenza virus strains by inhibiting cytokine production. These findings suggest that taurolidine may exhibit better chemotherapeutic properties in diseases where cytokines are the primary pathological component.

The tension of blood vessels is regulated by vascular smooth muscle signals. Previous studies have suggested that influenza virus infection can lead to pulmonary artery atherosclerosis [37]. Additionally, abnormal vascular smooth muscle signaling often leads to pulmonary hypertension [38], platelet aggregation [39], and atherosclerosis [40], suggesting that this signaling plays a crucial role in the anti-influenza virus response. Our results showed that taurolidine can inhibit the contraction of vascular smooth and improve the survival rate during infection with influenza virus, highlighting the importance of this signaling pathway in defending against influenza virus challenges. An interesting question is whether vascular endothelial cells or smooth muscle directly regulate the host immune response. Endothelial cells are involved in anti-inflammatory response [41], but further investigation is needed to determine how taurolidine influences endothelial cytokine production. Endothelial cells may regulate the production of cytokines in the lung through complex crosstalk mechanisms with epithelial cells or resident hematopoietic cells [42]. However, the identification of endothelial cells as the central coordinator of immune-mediated inflammation is of fundamental significance and has broad implications for the treatment of many diseases, such as influenza.

Furthermore, the etiology of several autoimmune diseases is directly related to inflammation response [43]. Therefore, it is important to understand the biological characteristics of taurolidine in regulating cytokine storm and developing appropriate chemical signaling transduction tools to identify specific molecular targets. This not only provides insights into the interaction between microorganisms and hosts, but also reveals potential new avenues for effective immunotherapy across a range of diseases. We also revealed that the administration of taurolidine reduced the release of Ca²⁺ after infection with the influenza virus. Since, vasoconstriction is regulated by Ca²⁺ concentration [44, 45]. This suggested that taurolidine may have the potential to treat other

diseases that depending on Ca²⁺-related signaling pathways. Importantly, these findings indicate that taurolidine might be a negative regulator of cytokine amplification and an activator of vascular smooth muscle signaling, potentially offering insights into how host genetic factors may influence survival advantages or disadvantages.

Conclusions

In summary, we demonstrated the antiviral ability of taurolidine. Our finding not only highlights the inhibitory effects of taurolidine on inflammatory response but also suggested its crucial role in vasoconstriction signaling. In addition, we revealed the potential of taurolidine-mediated mouse models in the treatment of influenza virus infections. Therefore, our study provides a theoretical basis for further research into the antiviral mechanism of taurolidine, suggesting its promising application for the prevention and treatment of influenza virus infections.

Supplementary Information The online version contains supplementary material available at <https://doi.org/10.1007/s00018-025-05636-6>.

Acknowledgements We are especially grateful to Wu Zhong at the Military Medical Research Institute for kindly providing the technical guidance, as well as to the Changchun Veterinary Research Institute (Biosafety Level III laboratory) for their experimental assistance.

Funding This work was supported by the Military Medical Research Institute Foundation project (grant number: AMMS-KYJJ-2022-014), the National Key Research and Development Program of China (2020ZX10001-016-003), and the National Key Research and Development Program of China (ZX10304402-003-006). This work was supported by a grant from National Key R&D Program of China (No. 2021YFC2301700) and the National Key Research and Development Program of China (No. 2020YFC0846100, 2023YFC0871000). This work was supported by Sichuan Province Science and Technology Department Project (grant number: 2024NSFSC0377), the project Science and Technology Bureau of Luzhou (Serial number: 00140094/41).

Availability of data and materials The datasets used and/or analysed during the current study are available from the corresponding author on reasonable request.

Declarations

Ethics approval and consent to participate The treatment of all mice was in accordance with the welfare and ethical guidance of Chinese laboratory animals (GB 14925–2001). The agreement was approved by the Animal Welfare and Ethics Committee of the Institute of Chinese Academy of Agricultural Sciences (permit number: SCXK-2012-017).

Consent for publication All authors consent to submit and publish this article.

Competing interests The authors declare that they have no known

competing financial interests or personal relationships that could have appeared to influence the work reported in this paper.

Open Access This article is licensed under a Creative Commons Attribution-NonCommercial-NoDerivatives 4.0 International License, which permits any non-commercial use, sharing, distribution and reproduction in any medium or format, as long as you give appropriate credit to the original author(s) and the source, provide a link to the Creative Commons licence, and indicate if you modified the licensed material. You do not have permission under this licence to share adapted material derived from this article or parts of it. The images or other third party material in this article are included in the article's Creative Commons licence, unless indicated otherwise in a credit line to the material. If material is not included in the article's Creative Commons licence and your intended use is not permitted by statutory regulation or exceeds the permitted use, you will need to obtain permission directly from the copyright holder. To view a copy of this licence, visit <http://creativecommons.org/licenses/by-nc-nd/4.0/>.

References

- García-Sastre A (2010) Influenza virus receptor specificity: disease and transmission. *Am J Pathol* 176(4):1584–1585
- Teijaro JR et al (2011) Endothelial cells are central orchestrators of cytokine amplification during influenza virus infection. *Cell* 146(6):980–991
- Hutchinson EC et al (2014) Conserved and host-specific features of influenza virion architecture. *Nat Commun* 5:4816
- Hurt AC et al (2012) Influenza antivirals and resistance: the next 10 years? *Expert Rev Anti Infect Ther* 10(11):1221–1223
- Miller MS, Palese P (2014) Peering into the crystal ball: in Uenza pandemics and vaccine efficacy. *Cell* 157(2):294–299
- Villalón-Letelier F et al (2017) Host cell restriction factors that limit influenza A infection. *Viruses* 9(12):1–18
- Teijaro JR et al (2014) Mapping the innate signaling cascade essential for cytokine storm during influenza virus infection. *Proc Natl Acad Sci U S A* 111(10):3799–3804
- Kobasa D et al (2007) Aberrant innate immune response in lethal infection of macaques with the 1918 influenza virus. *Nature* 445(7125):319–323
- Cantin AM et al (2015) Inflammation in cystic fibrosis lung disease: pathogenesis and therapy. *J Cyst Fibros* 14(4):419–430
- Liu Q et al (2016) The cytokine storm of severe influenza and development of Immunomodulatory therapy. *Cell Mol Immunol* 13(1):3–10
- Li QF, Tang DD (2009) Role of p47(phox) in regulating Cdc-42GAP, vimentin, and contraction in smooth muscle cells. *Am J Physiol Cell Physiol* 297(6):C1424–1433
- Dopico AM et al (2018) Calcium- and voltage-gated BK channels in vascular smooth muscle. *Pflugers Arch* 470(9):1271–1289
- Brozovich FV et al (2016) Mechanisms of vascular smooth muscle contraction and the basis for Pharmacologic treatment of smooth muscle disorders. *Pharmacol Rev* 68(2):476–532
- Quintavalle M et al (2011) Arterial remodeling and atherosclerosis: MiRNAs involvement. *Vascu Pharmacol* 55(4):106–110
- Ansari HR et al (2004) *Involvement of Ca²⁺ channels in endothelin-1-induced MAP kinase phosphorylation, myosin light chain phosphorylation and contraction in rabbit iris sphincter smooth muscle.* *Cell Signal* 16(5):609–619
- Arweiler NB et al (2012) Antibacterial effect of taurolidine (2%) on established dental plaque biofilm. *Clin Oral Invest* 16(2):499–504
- Egan BM et al (2002) Taurolidine attenuates the hemodynamic and respiratory changes associated with endotoxemia. *Shock* 17(4):308–311
- Bedrosian I et al (1991) Taurolidine, an analogue of the amino acid taurine, suppresses Interleukin 1 and tumor necrosis factor synthesis in human peripheral blood mononuclear cells. *Cytokine* 3(6):568–575
- Sima M et al (2023) Anti-inflammatory effects of theaflavin-3'-gallate during influenza virus infection through regulating the TLR4/MAPK/p38 pathway. *Eur J Pharmacol* 938:175332
- Qi J et al (2023) Schisandra chinensis (Turcz.) baill. Polysaccharide inhibits influenza A virus *in vitro* and *in vivo*. *FEBS Open Bio* 13(10):1831–1843
- Lv C et al (2023) Taurolidine improved protection against highly pathogenic avian influenza H5N1 virus lethal-infection in mouse model by regulating the NF-κB signaling pathway. *Virol Sin* 38(1):119–127
- Sakota Y et al (2014) Collagen gel contraction assay using human bronchial smooth muscle cells and its application for evaluation of inhibitory effect of formoterol. *Biol Pharm Bull* 37(6):1014–1020
- Jeon SB et al (2007) Flavone inhibits vascular contraction by decreasing phosphorylation of the myosin phosphatase target subunit. *Clin Exp Pharmacol Physiol* 34(11):1116–1120
- Görlach A et al (2015) Calcium and ROS: A mutual interplay. *Redox Biol* 6:260–271
- Pleschka S (2013) Overview of influenza viruses. *Curr Top Microbiol Immunol* 370:1–20
- van der Vries E et al (2013) Influenza virus resistance to antiviral therapy. *Adv Pharmacol* 67:217–246
- Hokschi B et al (2009) Taurolidine in the prevention and therapy of lung metastases. *Eur J Cardiothorac Surg* 36(6):1058–1063
- Kuiken T et al (2012) Pathogenesis of influenza virus infections: the good, the bad and the ugly. *Curr Opin Virol* 2(3):276–286
- Xia C et al (2018) Casein kinase 1α mediates the degradation of receptors for type I and type II interferons caused by hemagglutinin of influenza A virus. *J Virol* 92(7):e00006–e00018
- Rialdi A et al (2016) Topoisomerase I Inhibition suppresses inflammatory genes and protects from death by inflammation. *Science* 352(6289):aad7993
- Newton AH et al (2016) The host immune response in respiratory virus infection: balancing virus clearance and immunopathology. *Semin Immunopathol* 38(4):471–482
- de Jong MD et al (2006) Fatal outcome of human influenza A (H5N1) is associated with high viral load and hypercytokinemia. *Nat Med* 12(10):1203–1207
- Lee N et al (2007) Hypercytokinemia and hyperactivation of phospho-p38 mitogen-activated protein kinase in severe human influenza A virus infection. *Clin Infect Dis* 45(6):723–731
- Nara A et al (2015) An unusual autopsy case of cytokine storm-derived influenza-associated encephalopathy without typical histopathological findings: autopsy case report. *Am J Forensic Med Pathol* 36(1):3–5
- García-Ramírez RA et al (2015) IL6, and IL1B polymorphisms are associated with severe influenza A (H1N1) virus infection in the Mexican population. *PLoS ONE* 10(12):e0144832
- Sabbaghi A et al (2020) Role of gammadelta T cells in controlling viral infections with a focus on influenza virus: implications for designing novel therapeutic approaches. *Virol J* 17(1):174
- Peretz A et al (2019) Influenza virus and atherosclerosis. *QJM* 112(10):749–755
- Kovacs L et al (2019) PFKFB3 in smooth muscle promotes vascular remodeling in pulmonary arterial hypertension. *Am J Respir Crit Care Med* 200(5):617–627
- Fetalvero KM et al (2007) Cardioprotective Prostacyclin signaling in vascular smooth muscle. *Prostaglandins Other Lipid Mediat* 82(1–4):109–118

40. Bennett MR et al (2016) Vascular smooth muscle cells in atherosclerosis. *Circ Res* 118(4):692–702
41. Li M et al (2018) Pro- and anti-inflammatory effects of short chain fatty acids on immune and endothelial cells. *Eur J Pharmacol* 831:52–59
42. Sun X et al (2020) Crosstalk between endothelial cell-specific Calpain Inhibition and the endothelial-mesenchymal transition via the HSP90/Akt signaling pathway. *Biomed Pharmacother* 124:109822
43. Kirsch-Volders M et al (2020) Micronuclei, inflammation and auto-immune disease. *Mutat Res* 786:108335
44. Borysova L et al (2018) *Smooth muscle gap-junctions allow propagation of intercellular Ca^{2+} waves and vasoconstriction due to Ca^{2+} based action potentials in rat mesenteric resistance arteries.* *Cell Calcium* 75:21–29
45. Liu L et al (2019) *Comparison of Ca^{2+} Handling for the Regulation of Vasoconstriction between Rat Coronary and Renal Arteries.* *J Vasc Res* 56(4):191–203

Publisher's note Springer Nature remains neutral with regard to jurisdictional claims in published maps and institutional affiliations.